

## Physics at the closed shells

G de FRANCE

Grand Accélérateur National d'Ions Lourds (GANIL), BP 55027, F-14076 Caen Cedex 5, France

**Abstract.** Radioactive beams obtained via fragmentation of the projectile on a primary target have shown to be a powerful tool to produce exotic nuclei and some typical results obtained at GANIL in this area will be shown. To go further, and in particular, to get beams of exotic nuclei, new facilities have been developed recently. The physics expected from the use of these radioactive ion beam facilities is extremely ambitious as stated in the scientific motivations justifying their construction. At GANIL the SPIRAL facility is ready and will hopefully deliver the first radioactive beams in 2001. New experimental devices have been developed to fully exploit the potentiality expected from SPIRAL. EXOGAM is a new, efficient and powerful gamma ray spectrometer currently under installation at GANIL. The design and the performances expected from this array will be discussed.

**Keywords.** Gamma-ray; spectroscopy; magic numbers; exotic nuclei, EXOGAM.

**PACS Nos** 21.10.Hw; 21.10.Re; 23.20.Lv; 29.30.Kv

### 1. Introduction

Atomic and nuclear physics have always been looking to 'regularities' among the elements to get more insight in the understanding of nature. Today, as in the past, physics in the vicinity of magic numbers, their robustness as a function of mass, isospin and the search for new symmetry along the chart of nuclei is a major input for nuclear structure. This is true in a number of domain which I will describe in some more detail in the first part of this talk. In the second part, I will describe the new tools which are now mandatory in gamma-ray spectroscopy to go beyond what is feasible today. More precisely new arrays which are designed to work with radioactive beams are under construction. EXOGAM is one of these and I will use it as a typical example of these new tools.

### 2. Physics at the closed shells

#### 2.1 Identification of new magic elements

The discovery of new magic numbers is first of all mandatory to test and develop nuclear models. This is a basic milestone to understand the evolution of shell structure with exoticity. To get more detailed informations in terms of structure of these nuclei, it is necessary

to study the neighbouring nuclei of the magic elements. This is the case if one wants to learn about residual interactions.

The latest doubly magic elements discovered are  $^{100}\text{Sn}$  [5,6],  $^{78}\text{Ni}$  [8] and  $^{48}\text{Ni}$  [7].  $^{100}\text{Sn}$  is the heaviest  $N = Z$  doubly magic nuclei stable against  $p$ -emission from the ground state. The specific interest in the vicinity of this isotope is the study of  $p$ -rich nuclei and the stringent test of mass models. Mapping the  $p$ -drip line is also of prime importance to learn about  $rp$ -process and the associated waiting points. Just at the opposite,  $^{78}\text{Ni}$  is located in the  $r$ -process path region and it allows test of mass models in the neutron rich part of the chart. It is also the doubly magic nucleus which exhibits the largest  $A/Z$  ratio:  $A/Z = 2.79$ . Finally, the lately discovered  $^{48}\text{Ni}$  has several interesting properties. It first of all has the largest isospin projection  $T_z$  value ( $T_z = -4$ ) ever observed; it is also the unique element whose mirror nucleus ( $^{48}\text{Ca}$ ) is stable against particle emission, allowing therefore symmetry studies. The Ni isotope chain comprises 3 doubly magic nuclei ( $A = 48, 56, 78$ ), the two extremes having a difference of 30 neutrons. Finally, it is a good candidate together with  $^{45}\text{Fe}$  for direct  $2p$  emission from the ground state. This makes many good reasons to have a special look towards these magic elements.

The production method for these extremely rare nuclei consists in the high energy fragmentation of a beam onto a target. For  $^{100}\text{Sn}$  at GANIL, a beam of  $^{112}\text{Sn}$  at 63 MeV per nucleon was fragmented on a natural Ni target located between the two superconducting solenoids of the SSSI device (see [5]). The fragments are then selected first by standard alpha shape spectrometers, separated and identified in flight in the LISE spectrometer after a flight path of roughly 118 meters. The identification is made on the basis of redundant informations giving time of flight and energy loss in several detectors. After a drastic rejection of the events which do not match all the conditions, we get the usual energy loss versus time of flight plot also called identification plot.

It is interesting to see how far we can go with ‘only’  $4 \pm 2$  good events.  $^{48}\text{Ni}$  is calculated to be particle unstable by all common models. Even  $Z$  nuclei have a  $1p$  emission energetically forbidden as compared to  $2p$  emission in the very  $p$ -rich elements. Finally the  $Q$  values for  $2p$  emission  $Q(2p)$  are predicted to be between less than 1 MeV and more than 3 MeV corresponding to lifetimes between  $10^{-14}$  and 1 second! The plot of the expected half-life as a function of  $Q(2p)$  is given in figure 1 for a large number of usual models. Knowing the transmissions for  $^{48,49}\text{Ni}$  and the cross section decrease of  $\sigma(^{49}\text{Ni})/\sigma(^{48}\text{Ni}) \sim 26$ , we can deduce the number of counts expected for  $^{48}\text{Ni}$ :  $5.7 \pm 2.2$ . With a flight path of 118 m, (time of flight  $1.32 \mu\text{s}$ ) we are then able to estimate the lifetime for  $^{48}\text{Ni}$ :  $T_{1/2}(^{48}\text{Ni}) \sim 2.6_{-2.1}^{+\infty} \mu\text{s}$ .

Thus the lower limit at a  $1\sigma$  level is  $T_{1/2}(^{48}\text{Ni}) \sim 0.5 \mu\text{s}$  which translates to  $Q(2p) \sim 1.5$  MeV if we assume a spectroscopic factor of 1. These values lead to the experimental limits given in figure 1 which is a real test for the models. Indeed, models which have masses calculated explicitly for this mass region gives  $Q$  values closer to the present result than global models which lead to  $Q$  values larger than 1.5 MeV and therefore to much shorter half-lives. In the case of microscopic calculations, the results depend strongly on the parametrization of the Skyrme interaction.

The basic physics motivation in the search for new magic numbers and the associated test of the models is also at the origin of the quest for superheavy elements, where  $^{100}\text{Sn}$ ,  $^{48}\text{Ni}$ , and  $^{78}\text{Ni}$  test the isospin degree of freedom, the first ones in the  $p$ -rich direction,  $^{78}\text{Ni}$  in the  $n$ -rich one. Experiments on superheavy elements are aiming at exploring the next stable shell gaps. These elements are stabilized entirely by shell effects since their macroscopic

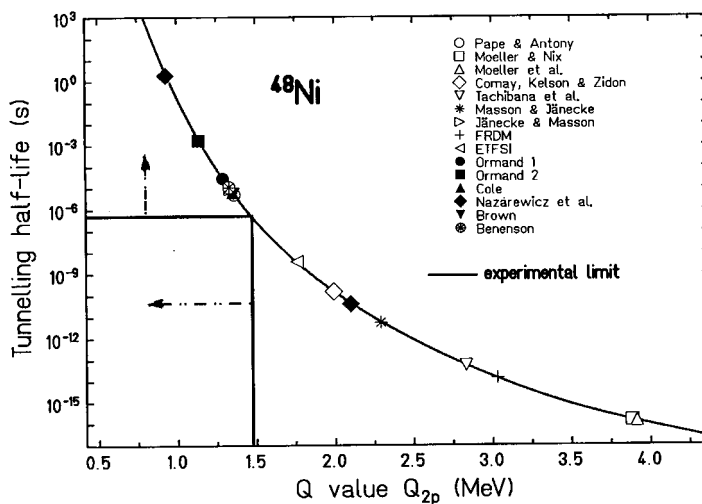


**Figure 1.** Barrier penetration half-life as a function of the two-proton  $Q$ -value.

energy becomes unstable with respect to shape deformation due to the strong Coulomb repulsion. The discovery of elements with  $Z = 100$  to  $Z = 112$  and today's controversy regarding the elements 114 [1], 116 [3,2] and 118 [3] indicates the tremendous activity in this quest and demonstrates the importance of this issue. Indeed, nuclei submitted to extreme conditions of excitation energy, spin, or isospin are of major importance to verify and improve the validity of nuclear models. Testing these models with nuclei having high charge and mass is equally fundamental.

Experimentally, very little is known about the structure of superheavy elements, except the  $\alpha$ -decay chains and estimates of the lifetimes. This lack of knowledge is a severe limitation when compared to model predictions which, in turn, limits the predictive power of the theoretical models. For example, basic features such as the position of the stabilizing spherical shell gap remains completely uncertain. The results from Nilsson–Strutinsky, Hartree–Fock or relativistic mean field theories vary strongly. While most of the calculations predict  $N = 184$  as the next spherical neutron gap, the different treatment of the large Coulomb potential and of the spin–orbit interaction leads to uncertainties in the position of proton shell gap, which could be located either at  $Z = 114$  (macroscopic–microscopic models) or at  $Z = 126$  (self-consistent calculations). It should also be noted that relativistic mean-field calculations predict  $Z = 120$  and  $N = 172$ . The different predictions are due to the fact that the gap at  $Z = 114$  originates from the spin–orbit splitting of the  $2f$  state, whereas the shell gap at  $Z = 120$  comes from the (smaller) splitting of the  $3p$  and  $2f$  states [4].

## 2.2 Spectroscopy of very heavy nuclei

Similar uncertainties are found in the transfermium region ( $Z < 100$ ) where also very little nuclear structure information is available. The physics case for spectroscopic studies

of these very heavy elements is the same as for the search for superheavy nuclei. Instead of reaching the orbitals generating the next spherical shell gaps directly with the number of particles in the system, we use the large quadrupole deformation which strongly influence these orbitals having a large intrinsic angular momentum. This causes the transfermium isotopes e.g. to occupy the same active orbitals as the spherical superheavy elements are expected to occupy. It is rather clear today that on the way to the spherical superheavy elements, a region of enhanced stability against fission is crossed (see for instance [9]). This gain in stability is attributed to a large quadrupole deformation ( $\beta_2 \sim 0.25-0.30$ ) especially around No isotopes. In-beam gamma-ray spectroscopy of  $^{254}\text{No}$  has been performed with the help of the recoil-decay-tagging technique [10,11]. Because of the four-fold magic character of the reaction used ( $^{48}\text{Ca} + ^{208}\text{Pb}$ ), leading to an exceptionally high cross section ( $3 \mu\text{b}$ ), indicating again the influence and importance of symmetry in the production mechanism, these studies have led to significant progress in the knowledge of the structure of these heavy nuclei. In the case of  $^{254}\text{No}$ , spins up to  $20^+$  have been established. In this region, and in particular for odd- $A$  nuclei, the high atomic number and low transition energies expected for the excited states lead to very high electronic conversion coefficients.

Recent macro-microscopic calculations with a Woods–Saxon potential [12] reproduce very nicely the extrapolated energy for the  $2^+$  state ( $E_{2^+} = 44 \text{ keV}$  (exp.),  $43 \text{ keV}$  (calc.)) and the quadrupole deformation ( $\beta_2 = 0.27$  (exp.),  $0.25$  (calc.)).

From this example we do see how spectroscopic studies of nuclei, which are produced with a rather large cross section as compared to those measured for spherical superheavy elements, contribute to the fundamental knowledge and understanding of the structure of nuclei that we cannot easily reach.

### 2.3 $\mu$ -second isomers

Another tool to study magicity are the  $\mu$ -seconds isomers. As already said, isomers are well understood in terms of shell model and strongly associated to the difference in the angular momenta ( $\Delta I$ ) of the final and initial states connected by  $\gamma$ -rays (or electrons), and thus to the spin-orbit term of the interaction. Around closed shells, the transitions are pure or have very small mixing. Measuring transitions which decay isomeric states in the vicinity of the closed shells, is therefore a particularly appropriate tool to have inputs relevant for the residual interactions and the nucleon effective charge.

These studies have been particularly prolific at GANIL using the LISE spectrometer as shown for example in [13]. In these experiments the recoiling ions are fully stripped which blocks the internal conversion channel and allow the flight of short-lived isomers over quite a long distance and small losses. The exotic ions are implanted in a silicon detector and the  $\gamma$ -rays decaying the isomeric level are detected by germanium (Ge) detectors surrounding the implantation detector.

As an example, we can mention the results obtained from the fragmentation of  $^{86}\text{Kr}$  at  $60.5 \text{ MeV/u}$  on a natural Ni target [14]. This experiment was aimed at looking at the isomers around the  $Z = 28$  shell gap. Several isomers have been identified and studied in some detail in  $^{78}\text{Zn}$  (see figure 2),  $^{80}\text{Ge}$ ,  $^{82}\text{Se}$ ,  $^{84}\text{Kr}$ , and  $^{86}\text{Sr}$ . In this region, the isomers are based on a 2 neutron hole configuration in  $g_{9/2}$  ( $\nu g_{9/2}^{(-2)}$ ). Shell model calculations using a realistic interaction [15] reproduce the spectra with a polarization of  $0.5e$  for both protons and neutrons (the effective charge is a measure of the polarization of the core induced by

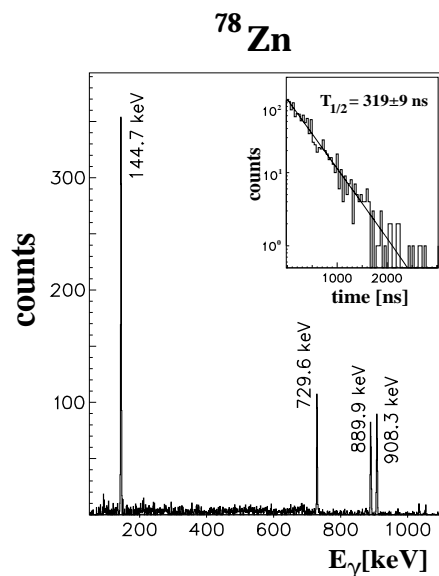


**Figure 2.**  $\gamma$ -ray spectrum of the isomeric state in  $^{78}\text{Zn}$ . The decay curve shown in the inset is summed over the four observed transitions.

the valence particle undergoing an electromagnetic transition). The  $8^+$  state is de-excited by an E2 transition ( $B(E2: 8^+ \rightarrow 6^+) = 1.21$  (5) Wu (1.06 Wu calc)).

From what we know in the  $^{100}\text{Sn}$  region and using symmetry arguments it is possible to deduce properties around the  $Z = 28$  shell gap [16,17]. Indeed,  $p$ -holes at  $N = 50$  and neutrons at  $Z = 28$  play a very similar role. In particular the relevant nuclei have an identical single particle structure around the Fermi surface: they are ‘valence mirror nuclei’ or more precisely they have the same structure at one major shell apart. The differences are twofold: (1) they have very different  $A/Z$  ratio (isospin) and (2) there is no overlap between neutrons and protons wave functions at  $Z = 28$  which also means no  $n$ - $p$  interaction. There is an  $8^+$  isomer in  $^{98}\text{Cd}$  which is associated to the existence of the  $N = 50$  shell gap.  $^{76}\text{Ni}$  is a 2 proton hole in  $^{78}\text{Zn}$  observed in this experiment. Therefore, the  $8^+$  isomer observed in  $^{78}\text{Zn}$  (maximum alignment in the  $\nu g_{9/2}^{(-2)}$  configuration), must be also present in  $^{76}\text{Ni}$  which is, in turn, a 2 neutron hole in  $^{78}\text{Ni}$ . From these symmetry based arguments it is possible to deduce that the existence of the observed isomer in  $^{78}\text{Zn}$  is evidence for the persistence of the  $Z = 28$  shell gap towards very neutron rich elements.

#### 2.4 Shape coexistence

It is predicted for quite a long time [18] that around  $A = 70$ – $80$ , shape coexistence should occur. A large variety of nuclear shapes is anticipated from the availability of several shell gaps. In particular the Kr isotopes are the best candidates. The equilibrium deformation is rather similar using Hartree–Fock + BCS, Nilsson–Strutinsky + BCS or Hartree–Fock–Bogolyubov calculations but the excitation energy for the shape coexisting states depends

on pairing interaction. The energy of low lying states is reasonably well known and enhanced B(E2) values are observed which correspond to the rotation of an elongated charge distribution with  $\beta \sim 0.35$ . However the level is more complicated than a simple rigid rotation, an observation which can be interpreted in terms of perturbation from shape co-existing states. To go beyond this assumption, it is therefore necessary to imagine more stringent test. This can be done by the determination of the electromagnetic transition probabilities and static moments of the low lying states i.e. the determination of the matrix elements associated to the decay.

To measure these probabilities, the basic idea is to avoid the *nuclear* interaction and deal only with the *Coulomb* part of the force. Experimentally, this can be done by performing a Coulomb excitation well below the Coulomb barrier. This reaction mechanism will excite the first  $2^+$  state which de-excite via gamma to the ground state. The matrix elements related to the decay of the first  $2^+$  state is related to the cross section of the excitation probability of this state ( $\sigma_{2+}$ ). However the  $Q_0$  moment perturbs the measurement. Other low lying collective states or change in the reduced B(E2) values can have similar effects. To eliminate these perturbation it is necessary to perform Coulomb excitation using several targets and to measure precisely the scattering angle dependence of ( $\sigma_{2+}$ ). Indeed, these measurements are significantly sensitive to  $Q_0$ . By giving the precise matrix elements, this sort of data is a very severe test for the current models and no doubt that sub-barrier Coulomb excitation experiment will be extremely interesting with the availability of radioactive beams.

### 2.5 Island of inversion

The last example which illustrates the importance and the relevance to date of the study of magic nuclei is related to what is called the ‘island of inversion’. Around  $N = 20$ , it is already known that there is a sudden change in the slope of the S2n plotted as function of mass and that the energy of the first  $2^+$  state is decreasing in Mg isotopes when the number of neutron increases between 14 and 20. Full shell model [20] calculations including both *sd* and *fp* shells have demonstrated that the  $N = 20$  gap is quenched between the  $1f7/2$  and the  $1d3/2$  orbitals which crosses each other around  $^{32}\text{Mg}$ . Hence it is called island of inversion. This quenching is due to an increasing mixing of the *fp* shell which is deformation driving. In  $^{32}\text{Mg}$ , only the first  $2^+$  state is known at 885 keV. An experiment has been performed at GANIL [21] to study in detail  $^{32}\text{Mg}$  (among others) and in particular to try to get information on the deformation. Gamma-ray spectroscopy has been made with a few number of Ge detectors. The challenge of this experiment is in the use of the in-beam spectroscopy, at the target point, of exotic nuclei produced in the high energy fragmentation of the beam. The fragments of interest had a velocity of about 30% of light velocity. In this experiment a second gamma ray line has been detected at 1430 keV. Unfortunately it was not possible to deduce the spin of the levels de-excited by this transition but it was shown that the 2 known lines are in coincidence. If it is a  $4+$ , then the ratio  $E(4+)/E(2+) = 2.6$  which is in between the value expected for a perfect rotor and perfect vibrator. This could be due to the role of the deformation induced by the *fp* shell mixing.

Several examples that I have described here deal with spectroscopy and the level of precision and efficiency which is needed today requires high performance detectors. This

is even more important for future studies related to the advent of radioactive beams such as those expected from the SPIRAL facility at GANIL. In the following section, I will describe in some detail EXOGAM, one of the gamma-ray arrays of the new generation which is specifically designed to work with radioactive beams.

### **3. The EXOGAM array**

#### *3.1 Design specifications*

Radioactive beams impose new design considerations to a  $\gamma$ -ray spectrometer. The beam intensity is expected to be much lower than with stable beams, factor of 10 or even 1000 lower. EXOGAM must therefore be designed to maximize the total photopeak efficiency. In maximizing efficiency the spectrum quality must be maintained. The spectrum quality is determined by the peak to total ratio and energy and time resolution. The total efficiency measures the ability of the array to collect statistics. The spectrum quality measures the effectiveness of the array in isolating a single sequence or sequences of gamma-rays from a complex spectrum.

There will be a large variety of nuclear reactions using radioactive beams on which the design of a detection system must be based. The experimental conditions will be very different from one experiment to another in terms of  $\gamma$ -ray energy (from x-rays of tens of keV to  $\gamma$ -ray energies up to 5–6 MeV), of multiplicity (from one to  $\sim 15$  coincident photons); of recoil velocity (from zero to  $\sim 10\%$  of light velocity); and of kinematics of the reaction mechanism (from recoiling fusion products emitted at  $\sim 0^\circ$  or scattered particles between  $0^\circ$  and  $180^\circ$ ). This variety means that the set up of the array must be adapted for each experiment. The radioactive nature of the beam is also a concern and shielding of the detectors becomes an important design criterion.

It is also clear that in addition to the detection of gamma radiation it will be vital to have ancillary detectors available to detect both light and heavy charged particles and neutrons.

#### *3.2 Segmented Clover Ge detector*

In order to meet all the design criteria the EXOGAM spectrometer will consist of an array of high resolution germanium detectors each surrounded by an escape suppression shield.

One composite and segmented detector is the segmented Clover detector (see [22] for a detailed description). It is made of four individual crystals each electronically segmented into four regions. The EXOGAM array will consist of segmented Clover detectors. This segmentation is particularly useful when the emitting nuclei recoil with a large velocity since it allows a better determination of the interaction point of the  $\gamma$  ray in the detector. The detectors can be easily arranged in different configurations as will be shown later. This high degree of versatility is a very important design criterion as in the future the full gamut of nuclear reactions with stable and radioactive beams will be used for nuclear spectroscopy.

GEANT simulation calculations have been carried out to optimize the performances of Clover detectors for EXOGAM. The EXOGAM Clover will be based on the use of large Ge crystals, 60 mm in diameter and 90 mm long, before shaping. The photopeak efficiency

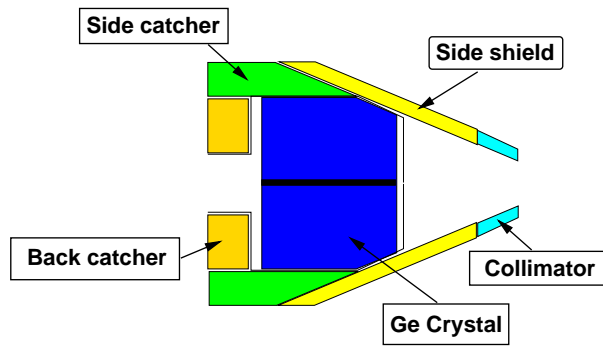


**Figure 3.** The different elements of the BGO suppression shield for the segmented Clover Ge detectors (not to scale).

of each Clover will be  $\epsilon_p \omega \sim 12 \times 10^{-3}$  at 11 cm for a 1.3 MeV  $\gamma$ -ray. The segmentation of the crystals leads to a reduction by a factor of two of the Doppler broadening of the peak as compared to a non-segmented crystal.

### 3.3 Suppression shield for a segmented Clover Ge detector

Each segmented Clover Ge detector is surrounded by an escape suppression shield. The shield designed for the EXOGAM Clover is based on a new concept in which the shield comprises several distinct elements (figure 3), a backcatcher, a rear side element and a side shield (see [23] for details). Designing suppression shields in this way, from individual elements, creates greater flexibility for different configurations. The shields will be operated in two configurations. The first is with the back catcher and rear-side element, configuration A, and the second with the additional side elements, configuration B.

### 3.4 Segmented Clovers arrays

The EXOGAM segmented Clovers can be arranged in different geometries. In all the geometries the suppression elements can be used in configurations A and B. Configuration A is the close packed geometry where the Ge detectors can essentially touch at the front. Configuration B is the pulled back geometry in which the detectors are further from the target to allow for the inclusion of the additional side suppression elements. An array geometry for the Clovers to be as close as possible to the target is with the detectors on the faces of a cube. An array of 16 Clover detectors can be arranged. An isometric projection of the array is shown in figure 4. In configuration A the signals from adjacent Ge crystals can be summed to increase the efficiency. The calculated increase in efficiency is 6%.

The configurations, distances from the target, and performances for arrays of segmented Clovers are summarized in table 1.

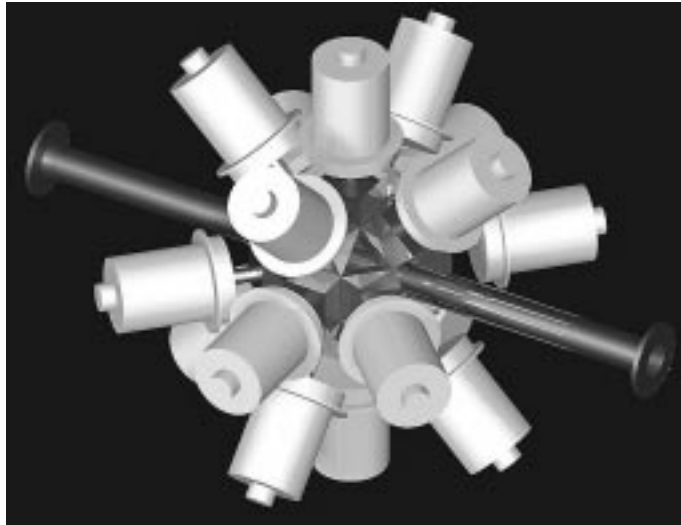


**Figure 4.** The EXOGAM spectrometer with 16 segmented Clovers.

**Table 1.** Summary of array geometries for segmented Clovers.

Geom.	Shield conf.	$d$ Ge-target (mm)	Phot. eff.		Peak/Total	
			662 keV	1.3 MeV	662 keV	1.3 MeV
Cube	B	68.3	0.15	0.10	0.72	0.60
16 det.	A	114.1	0.28	0.20	0.57	0.47
16 det.	B	147.4	0.17	0.12	0.72	0.60

#### 4. Conclusions

With the development of radioactive beams in several places all over the world and the associated new spectrometers, the limits of our current knowledge in nuclear structure will be overtaken. More than a conclusion, I hope that this new step will bring a harvest of surprise.

#### Acknowledgement

I would like to thank all the people who have contributed to this lecture.

#### References

- [1] Y T Oganessian *et al*, *Phys. Rev. Lett.* **83**, 3154 (1999)
- [2] Y T Oganessian *et al* (private communication)
- [3] V Ninov *et al*, *Phys. Rev. Lett.* **83**, 1104 (1999)

- [4] K Rutz *et al*, *GSI Annual Report*, (1999) 38  
M Bender *et al*, in preparation
- [5] M Lewitowicz *et al*, *Phys. Lett.* **B332**, 20 (1994)
- [6] R Schneider *et al*, *Z. Phys.* **A348**, 241 (1994)
- [7] B Blank *et al*, *Phys. Rev. Lett.* **84**, 1116 (2000)
- [8] Ch Engelmann *et al*, *Z. Phys.* **A352**, 351 (1995)
- [9] G Muenzenberg *et al*, *Z. Phys.* **A322**, 227 (1985)
- [10] M Leino *et al*, *Europhys. J.* **A6**, 63 (1999)
- [11] P Reiter *et al*, *Phys. Rev. Lett.* **82**, 509 (1999)
- [12] I Muntian, Z Patyk and A Sobiczewski *et al*, *GSI Annual Report*, (1999) 39
- [13] R Grzywacz *et al*, *Phys. Rev.* **C55**, 1 (1997)
- [14] J M Daugas *et al*, *Phys. Lett.* **B476**, 213 (2000)
- [15] Sinatkas *et al*, *J. Phys. G: Nucl. Part. Phys.* **18**, 1377, 1401 (1992)
- [16] R Grzywacz *et al*, *Phys. Rev. Lett.* **81**, 766 (1998)
- [17] M Gorska *et al*, *Phys. Rev. Lett.* **79**, 2415 (1997)
- [18] W Nazarewicz *et al*, *Nucl. Phys.* **A435**, 397 (1985)
- [19] R Bengtsson, *Nuclear structure of the zirconium region* (Springer, 1985) 17
- [20] N Fukunishi *et al*, *Phys. Lett.* **B296**, 279 (2000)
- [21] M J Lopez, PhD thesis, GANIL T 00 01
- [22] G Duchêne *et al*, *NIM* **A432**, 90 (1999)
- [23] J Simpson *et al*, *Heavy ion physics* **11**, 159–188 (2000)